International Journal of Mining Science and Technology 35 (2025) 1775–1788

Contents lists available at ScienceDirect

International Journal of Mining Science and Technology

journal homepage: www.elsevier.com/locate/ijmst

# Reverse floc-flotation of talc from chalcopyrite by using polyvinyl acetate as a flocculant: Adsorption and bubble capture studies

Yu Xie [a,b], Wanzhong Yin [b,c], Qi Liu [a,*], Daowei Wang [a], Wenju Sun [b]

[a] Department of Chemical and Materials Engineering, University of Alberta, Edmonton T6G 1H9, Canada
[b] School of Resources and Civil Engineering, Northeastern University, Shenyang 110819, China
[c] State Key Laboratory of Mineral Processing, Northeastern University, Shenyang 110819, China

ARTICLE INFO

*Article history:*
Received 28 May 2025
Received in revised form 28 August 2025
Accepted 31 August 2025
Available online 30 October 2025

*Keywords:*
Chalcopyrite
Ultrafine talc
Polyvinyl acetate
Floc-flotation
Flocculant adsorption
Bubble capture

ABSTRACT

Chalcopyrite is often intergrown with talc, which, after grinding, forms ultrafine particles (<10 μm) that readily coat chalcopyrite surfaces, hindering flotation and causing significant losses in tailings. This study evaluates polyvinyl acetate (PVAc), a thermoplastic polymer, as a selective flocculant to enhance reverse flot ation separation of chalcopyrite from ultrafine talc. Flotation tests showed that at a PVAc dosage of 40 mg/L, talc can be effectively and selectively removed, enabling efficient separation. Laser particle size analysis and scanning electron microscopy-energy dispersive spectrometry (SEM-EDS) confirmed that PVAc promotes selective talc aggregation without affecting chalcopyrite. X-ray photoelectron spectroscopy (XPS) and density functional theory (DFT) calculations revealed that hydrogen bonding between PVAc ester groups and surface hydroxyls on talc drives the flocculation, while chalcopyrite lacks suitable binding sites. PVAc adsorption also enhances talc hydrophobicity. Furthermore, particle-bubble coverage angle measurements and extended Derjaguin-Landau-Verwey-Overbeek (DLVO) theory theoretical calculations demonstrated that PVAc-induced flocculation increases attractive interactions between talc and bubbles, shifting the total interaction energy from repulsive to attractive and promoting bubble-particle attachment. This study clarifies the selective adsorption and flocculation mechanisms of PVAc and reveals the coupling of flocculation and flotation of ultrafine talc from a particle-bubble capture perspective, while expanding the potential of ester-based polymers for ultrafine mineral recovery.



## 1. Introduction

Ultrafine mineral particles, typically defined as those with particle sizes smaller than about 10 μm, are difficult to effectively recover and utilize during mineral processing and separation due to their small sizes. These particles cannot be efficiently recovered by froth flotation and are often discarded to tailings [1]. Tailings are the leftover waste materials after ore beneficiation and commonly contain pollutants such as heavy metals, acid-generating sulfide gangue, and chemical reagents. Long-term accumulation of wet fluid tailings poses severe environmental threats, including water pollution, air pollution, soil contamination, ecological damage, and potential geological hazards. The abandonment and storage of ultrafine minerals constitute latent pollution sources, posing a threat to human life.

In terms of the separation of ultrafine minerals, traditional methods such as gravity separation, magnetic separation, and conventional froth flotation are generally not effective. In contrast, floc-flotation has emerged as one of the most efficient approaches for recovering ultrafine minerals. This technique relies on the adsorption of polymeric flocculants to the mineral surface, where the polymers' bridging action promotes the aggregation of ultrafine particles into larger flocs, thus enhancing flotation performance [2]. Floc-flotation not only enhances the separation of ultrafine minerals, but also mitigates their environmental impact and contributes to resource recovery. By optimizing the choice of flocculants and flotation conditions, it is possible to improve mineral separation efficiency, reduce environmental contamination, and achieve more sustainable mineral resource recovery and tailings management.

However, this technology still faces challenges, particularly in the selection of suitable flocculants. Traditional flocculants, such as polyacrylamide, are hydrophilic, leading to strong repulsive interactions between the resulting flocs and air bubbles, thereby reducing the flotation efficiency of ultrafine minerals. It is well

* Corresponding author.
*E-mail address:* yinwanzhong@mail.neu.edu.cn (W. Yin).

https://doi.org/10.1016/j.ijmst.2025.08.016
2095-2686/

known that ester groups (–COOR) are classic hydrophobic functional groups, widely used in the production of plastics and waterproof materials due to their hydrophobicity [3]. Employing ester-containing polymers as flocculants for ultrafine minerals could substantially enhance flotation efficiency. Polyvinyl acetate (PVAc), a thermoplastic polymer rich in ester groups, is commonly used in adhesives, coatings, and pharmaceuticals [4]. PVAc is the esterification product of polyvinyl alcohol (PVA), as shown in Eq. (1) [5].

$$-[CH_2-CH(OH)]_n + nCH_3COOH \xrightarrow{\text{Acidcatalysis}} -[CH_2-CH(OCOCH_3)]_n + nH_2O \quad (1)$$

PVA is a polymer rich in hydroxyl groups (–OH) and exhibits strong hydrophilicity. After esterification, most of the hydroxyl groups are converted into ester groups, significantly enhancing the hydrophobicity of the polymer. This transformation makes PVAc a highly promising candidate as a selective flocculant. Nevertheless, no studies have been reported on the application of PVAc as a flocculant in the flotation of ultrafine minerals.

Talc has a Mohs hardness of 1 and is one of the softest minerals in nature. It is commonly associated with chalcopyrite. During grinding and separation processes, talc is often over-ground, forming ultrafine particles smaller than 10 μm [6]. These ultrafine talc particles tend to coat the surface of chalcopyrite, forming "slime coating" that hinders the adsorption of collectors (e.g., xanthates), thereby reducing chalcopyrite flotation recovery. As a result, large quantities of chalcopyrite and ultrafine talc are lost together to the tailings [7]. Through reverse floc-flotation, talc can be removed from chalcopyrite ores. This not only reduces tailings volume but also mitigates the pollution of water and soil caused by tailings accumulation.

The present study investigated the selective floc-flotation of ultrafine talc from chalcopyrite using PVAc as a flocculant in a reverse flotation system. The flocculation performance of PVAc on chalcopyrite and ultrafine talc was examined through laser particle size analysis and scanning electron microscopy-energy dispersive spectrometry (SEM-EDS). X-ray photoelectron spectroscopy (XPS) and density functional theory (DFT) calculations were employed to elucidate the mechanism underlying the selective adsorption of PVAc on chalcopyrite and ultrafine talc. In addition, bubble-particle interaction mechanisms are analyzed through coverage angle measurements and extended Derjaguin-Landau-Verwey-Overbeek (DLVO) theory calculations before and after talc flocculation, thereby providing an in-depth theoretical understanding of the coupling mechanism between flocculation and flotation.

## 2. Materials and methods

### 2.1. Minerals

In this work, bulk samples of high-purity chalcopyrite and talc were acquired from Kunming in Yunnan Province and Anshan in Liaoning Province, China, respectively. Their mineral phases were analyzed by X-ray diffraction (XRD), and the corresponding patterns are presented in Fig. 1. The diffraction data confirmed the high purity of both samples, with no secondary phases detected. Chemical composition assessments indicated that the chalcopyrite and talc samples possessed purities of 98.18% and 92.03%, respectively. The raw minerals were used after crushing, grinding, and sieving. Chalcopyrite particles within the –74+38 μm range and talc particles below 10 μm were employed for flotation studies. For mechanistic investigations, both minerals were further milled to obtain particles under 5 μm, which were then used for subsequent research work [8].

### 2.2. Reagents

In the flotation experiments, dodecylamine (DDA, AR, 98%) was employed as a collector for talc, and potassium permanganate ($KMnO_4$, AR, 95%) was used as a depressant for chalcopyrite. Hydrochloric acid (HCl) and sodium hydroxide (NaOH) were used for pH adjustment. All reagents were provided by China National Pharmaceutical Group Chemical Reagent Co., Ltd., and all experiments were conducted using deionized water. Polyvinyl acetate (PVAc, AR, 94%), obtained from Macklin Biochemical Co., Ltd., was selected as the flocculant. To prepare the PVAc solution, anhydrous ethanol and deionized water were mixed in a 1:1 ($v/v$) ratio as the solvent, followed by heating and stirring to ensure complete dissolution. The polymer PVAc is mainly composed of three elements: C, H, and O, with its molecular structure depicted in Fig. 2. The polymer's backbone primarily includes ester groups, alkyl chains, and carbon chain segments [9].

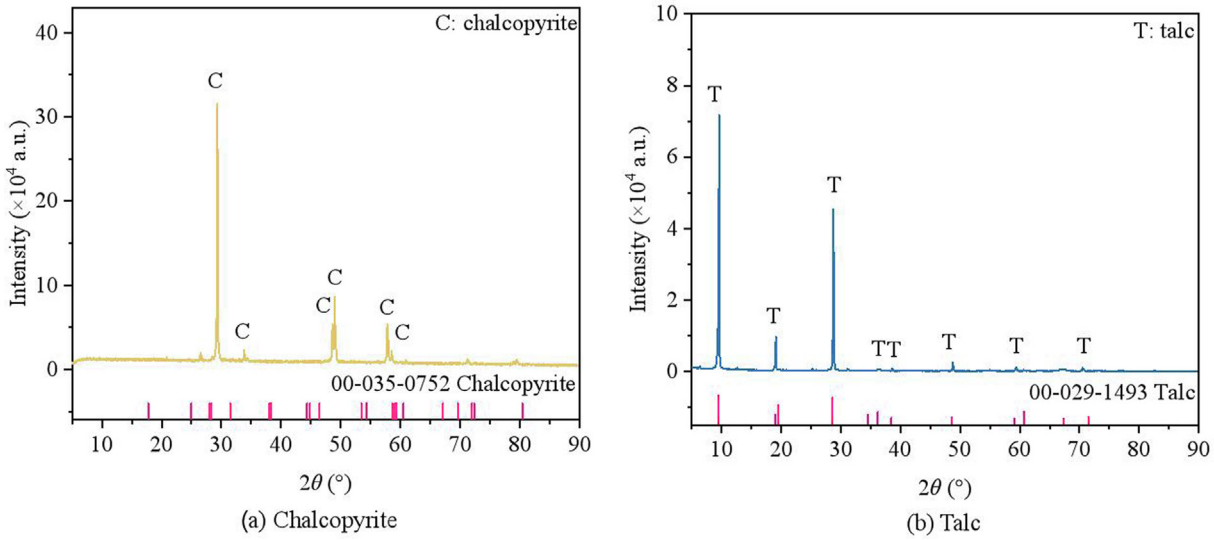


**Fig. 1.** XRD patterns of mineral sample of chalcopyrite and talc.

### 2.3. Micro-flotation experiment

Flotation experiments were conducted for both individual chalcopyrite and talc minerals, as well as their mixtures, using an XFG flotation machine (Fig. S1 in Supplementary materials). Initially, 2 g of the mineral sample was weighed and combined with 40 mL deionized water, after which the slurry was agitated at 1992 rpm [10]. Pulp pH was adjusted by adding HCl or NaOH, followed by the sequential introduction of PVAc, $KMnO_4$, and DDA, with each addition being stirred for 3 min. After adding reagents, the flotation was carried out by scraping the froth for 3 min, which was dried and weighed to determine flotation recovery.

In the flotation experiment of artificial mineral mixtures, the recovery of copper in the mixed mineral systems was calculated by examining the copper concentration in the concentrate. The copper concentration was determined by XRF following high temperature fusion of the concentrate with fluxing reagents. Additionally, flotation performance was evaluated using the enrichment ratio, defined as the ratio of concentrate grade to feed grade [11]. Each experiment was performed in triplicate, and the mean value was reported as the final result [12].

### 2.4. Analysis methods

#### 2.4.1. Laser particle size measurements

The particle size distributions of chalcopyrite and talc, before and after interacting with the flocculant PVAc, were measured by a Malvern 3000 laser particle size analyzer (UK). To prepare the mineral suspensions, chalcopyrite and talc were processed separately under flotation conditions, with PVAc added to facilitate effective interaction with the minerals. A rubber-tipped dropper was then used to transfer a small quantity of the well-dispersed slurry into the measurement cell. Particle/floc size distributions were recorded once the sample concentration met the required specifications for analysis [13].

#### 2.4.2. SEM-EDS measurements

Changes in the aggregation state of chalcopyrite and ultrafine talc particles resulting from PVAc interaction were investigated via SEM-EDS. This was also used to determine the elemental distribution on the mineral surfaces. Based on the flotation tests, mineral particles after treatment by PVAc were filtered and air-dried under natural conditions. The dried mineral samples were then sputter-coated with gold and analyzed by a ZEISS Sigma 300 scanning electron microscope [14].

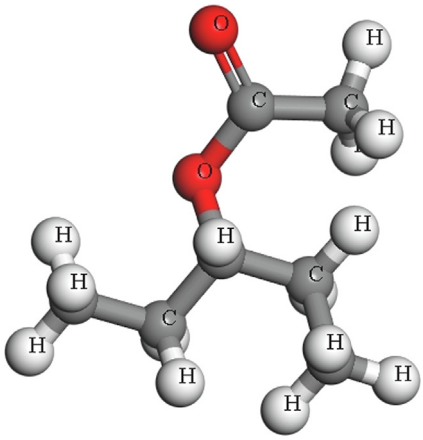


**Fig. 2.** Molecular structure of PVAc.

#### 2.4.3. XPS measurements

Based on flotation test conditions, uniformly dispersed chalcopyrite and ultrafine talc slurries were separately prepared, and PVAc was added to the slurry to ensure complete interaction with the mineral surfaces. The slurries were then filtered, and the collected mineral samples were dried in a vacuum oven. XPS analysis was performed using a thermo scientific spectrometer (USA) operated at 12 kV and 200 W. The binding energies were calibrated against the C 1s peak at 284.80 eV. This procedure was employed to investigate the adsorption behavior of PVAc on the surfaces of chalcopyrite and ultrafine talc.

#### 2.4.4. First-principle calculations

The adsorption energy serves as a crucial parameter for evaluating the binding strength of PVAc molecules at the mineral surfaces. Optimization of the initial unit cells of chalcopyrite and talc was performed by CASTEP unit in the course of the simulation [15]. The PW91 functional was employed to model the electronic exchange-correlation, with a plane-wave cutoff energy set at 340 eV and a Brillouin zone *K*-point grid of 1×1×2. Given that PVAc is a high-molecular-weight polymer comprising numerous repeating units, the calculations were also carried out using the CASTEP module. Here, selected segments of the PVAc macromolecular chain were used for simulation optimization to streamline the computational process. The geometric optimization of both the mineral surfaces and reagent molecules adhered to the following convergence criteria: (a) maximum force of 0.03 eV/Å; (b) maximum stress of 0.1 GPa; and (c) maximum displacement of 0.002 Å.

According to literature, the (112) surface of chalcopyrite and the (001) surface of talc exhibit the lowest surface energies, making them the most commonly exposed facets of these minerals. Consequently, for the calculation of PVAc adsorption energy, the (112) surface was selected for chalcopyrite, while the (001) surface was chosen for talc. A vacuum layer of 20 Å along the *Z*-axis was applied, and periodic structures were constructed using 3×2 supercell models for chalcopyrite and 3×1 supercell models for talc [16]. The adsorption energy of PVAc at the mineral surfaces was determined as follows:

$$\Delta E = E_{\text{total}} - (E_{\text{mineral}} + E_{\text{reagent}}) \quad (2)$$

where $\Delta E$ represents the adsorption energy of the PVAc molecule on the chalcopyrite (112) surface or talc (001) surface; $E_{\text{mineral}}$ and $E_{\text{reagent}}$ the energies of the mineral surface model and the PVAc molecule, respectively; and $E_{\text{total}}$ the total energy of their combined system.

#### 2.4.5. Measurement of coverage angle between particles and bubbles

In this study, a custom-designed coverage angle measurement device was utilized to assess the capture efficiency between ultrafine talc particles and bubbles, before and after PVAc flocculation. A schematic of the device is shown in Fig. S2. Following the flotation procedure, 2 g of ultrafine talc particles were dispersed uniformly in 40 mL of deionized water for the experiment, and two types of dispersed ultrafine talc slurries were prepared using a flotation machine. An appropriate amount of PVAc was then added to one of the slurries to ensure complete interaction between PVAc and talc, resulting in the formation of a flocculated slurry. The coverage angle measurement device was then used to introduce a bubble into the slurry, which was stirred at a low speed to allow continuous collisions between the mineral particles and bubbles. Images were captured at 15 and 30 s intervals, showing the talc particles adhering to the surface of the bubbles. The coverage angle between

the ultrafine talc particles (or flocs) and the bubbles was subsequently quantified using ImageJ software.

## 3. Results and discussion

### 3.1. Micro-flotation experimental results

#### 3.1.1. Flotation results of single mineral

To suppress chalcopyrite, $KMnO_4$ was selected as the inhibitor in the flotation experiment. Fig. 3a illustrates the flotation performance of chalcopyrite and ultrafine talc when PVAc is present. As observed in Fig. 3a, $KMnO_4$ effectively suppresses chalcopyrite flotation, with recovery rates consistently remaining below 15%, regardless of the addition of PVAc, when DDA is used as the collector. This inhibition is attributed to the redox reaction between $KMnO_4$ and chalcopyrite, which results in the oxidation of chalcopyrite and significantly hampers its flotation, as confirmed in previous studies. By comparison, $KMnO_4$ shows negligible impact on ultrafine talc flotation. With an increase in DDA concentration, the talc flotation recovery exhibits an upward trend. However, despite the increase in DDA concentration, the overall recovery remains below 60%, which is significantly lower than the typical flotation recovery levels for talc. This is primarily due to the extremely fine particle size of talc (below 10 μm), which impedes effective collision and adhesion to air bubbles during flotation. However, the addition of PVAc leads to a substantial increase in talc flotation recovery. This suggests that PVAc can effectively flocculate the ultrafine talc particles, thereby increasing their apparent particle size, enhancing their interaction with bubbles, and enabling their adhesion to the bubbles, facilitating their transport to the surface.

For a more comprehensive analysis of the influence of PVAc concentration on flotation outcomes, additional experiments were conducted, and the results are displayed in Fig. 3b. As indicated by Fig. 3b, it is evident that with an increase in PVAc concentration, there is little alteration in the flotation recovery of chalcopyrite, while the flotation recovery of talc continues to show an upward trend. This evidences that PVAc plays a crucial role in improving the floatability of ultrafine talc particles [17]. Upon reaching a PVAc concentration of 40 mg/L, the talc flotation recovery reaches 93.30%. However, when the concentration of PVAc is further increased, the flotation recovery of talc begins to decrease. This decline in recovery is likely due to excessive flocculation, where the talc particles aggregate too much, result-

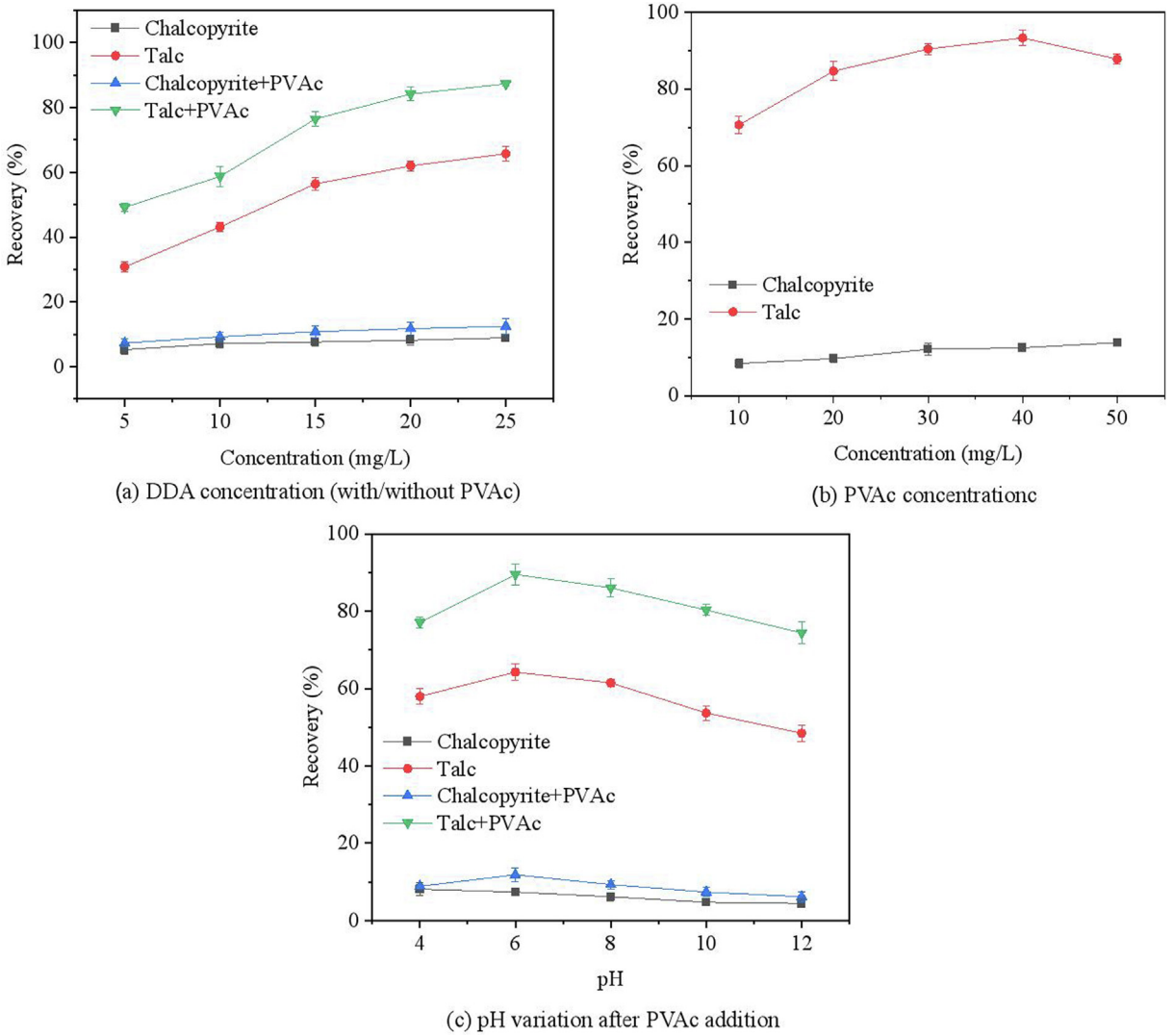


**Fig. 3.** Flotation performance of chalcopyrite and ultrafine talc under different conditions (pH: 7, DDA: 20 mg/L, PVAc: 20–40 mg/L, and $KMnO_4$: 150 mg/L).

ing in an increase in their size beyond the optimal range for flotation [18].

The relationship between slurry pH and the flotation performance of chalcopyrite and ultrafine talc in the presence of PVAc was investigated, and the results are shown in Fig. 3c. As illustrated in Fig. 3c, talc flotation is most favorable at pH 6, while its recovery decreases under strongly acidic or alkaline conditions. The decrease in flotation recovery is related to the hydrolysis of PVAc under strong acidic and strong alkaline conditions, whereby PVAc is converted into polyvinyl alcohol [19]. The resulting polyvinyl alcohol has a certain degree of hydrophilicity, which inhibits the flotation of talc. Notably, the flotation difference between chalcopyrite and talc is most pronounced at pH 8. Under this condition, the recovery of chalcopyrite drops significantly to only 8.40%, whereas the recovery of ultrafine talc reaches 84.50%. Separation in acidic environments is less effective, as $KMnO_4$ exhibits stronger oxidative depression on chalcopyrite under alkaline conditions.

### 3.1.2. Flotation results of artificial mineral mixtures

A mixture of chalcopyrite and ultrafine talc at a 3:2 mass ratio was precisely prepared to evaluate the impact of the flocculant PVAc on their floc-flotation behavior.

Flotation separation experiments were conducted on this binary mixture under the defined experimental conditions. The results are presented in Fig. 4. In accordance with Fig. 4, when PVAc is absent, the chalcopyrite concentrate exhibited a relatively low copper grade and recovery rate, with values of only 23.78% and 23.60%, respectively. The enrichment ratio was calculated to be a mere 1.32, indicating that the flotation separation efficiency was low. These results suggest that, without the presence of PVAc, the ultrafine talc particles in the mineral mixture were not effectively separated or removed during the flotation process. In contrast, when PVAc was introduced as a flocculant, the ultrafine talc particles were efficiently removed from the flotation system, thereby allowing for a more effective separation of the minerals. As a result, the copper grade in the chalcopyrite concentrate increased significantly to 31.61%, and the recovery increased to 92.20%. Moreover, the enrichment ratio was increased to 1.76, demonstrating a substantial improvement in flotation efficiency. Therefore, it can be concluded that PVAc is an efficient flocculant for the separation of chalcopyrite from ultrafine talc.

### 3.2. Selective flocculation analysis of PVAc

To investigate the flocculation effect of PVAc on chalcopyrite and ultrafine talc, the impact of PVAc on the overall particle size distribution of both minerals was systematically evaluated. The particle size distributions of chalcopyrite and ultrafine talc, before and after PVAc treatment, are presented in Fig. 5. According to Fig. 5, the average particle size of talc prior to PVAc treatment was 7.34 μm. Following the addition of PVAc, the ultrafine talc was aggregated, leading to a substantial increase in the average particle/floc size to 33.74 μm [20]. This indicates that PVAc effectively promoted the aggregation of ultrafine talc, forming larger flocs. In contrast, the effect of PVAc on chalcopyrite was minimal. Prior to PVAc treatment, the average particle size of chalcopyrite was 63.26 μm, which increased only slightly to 65.40 μm after the addition of the flocculant. This minimal change in the particle size of chalcopyrite suggests that PVAc does not have a significant impact on the aggregation of chalcopyrite particles. This outcome highlights the strong selective flocculation capability of PVAc, which can preferentially aggregate talc particles, thereby improving their separation efficiency in flotation processes.

### 3.3. Analysis of SEM-EDS results

The investigation of modifications in the surface morphology of mineral particles during flotation is crucial for gaining a comprehensive understanding of the flotation process, as the surface characteristics of the particles play a significant role in the efficiency of separation. To evaluate these changes, SEM-EDS were employed to evaluate the surface morphology of chalcopyrite and ultrafine talc prior to and following interaction with the flocculant PVAc. The results are presented in Figs. 6 and 7.

As shown in Fig. 6a1, the natural chalcopyrite particles exhibit an irregular pyramidal shape, with a relatively sparse distribution across the surface. This characteristic indicates that the chalcopyrite particles are not highly aggregated in their natural state. After interacting with PVAc, as shown in Fig. 6b1, only a small amount of fine particles were adsorbed on the surface of the chalcopyrite, and the chalcopyrite particles did not aggregate significantly. Their distribution remained sparse, similar to their natural state.

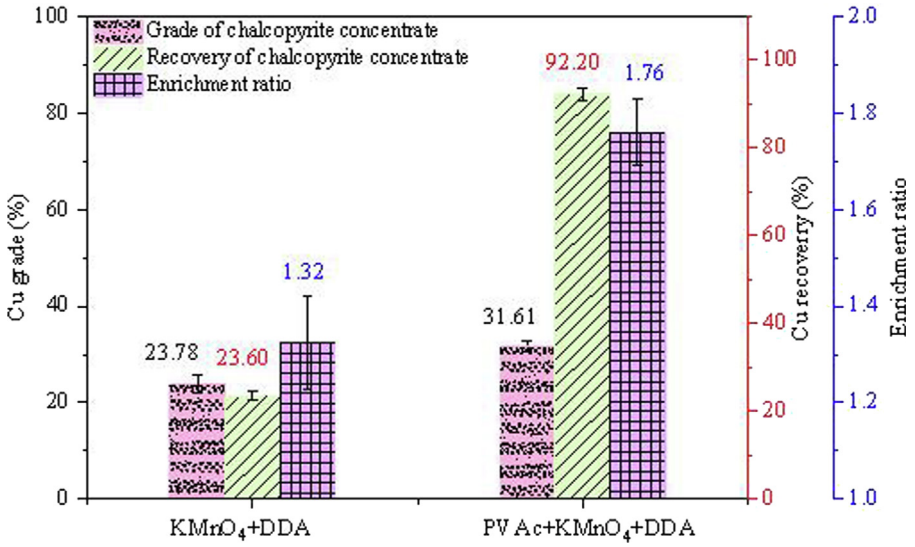


**Fig. 4.** Flotation separation performance of PVAc on a chalcopyrite and ultrafine talc mixture (pH: 8, PVAc concentration: 40 mg/L, $KMnO_4$: 150 mg/L, and DDA: 20 mg/L).

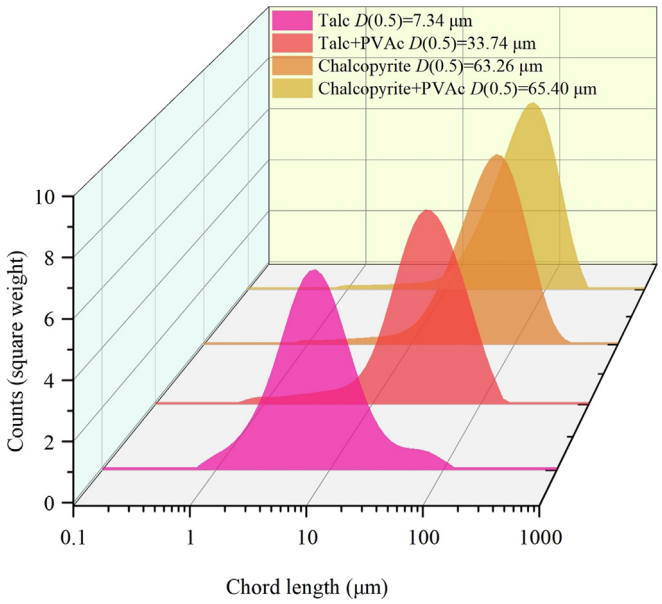


**Fig. 5.** Laser particle size distribution of chalcopyrite and ultrafine talc before and after adding PVAc (pH: 8, and PVAc: 40 mg/L). Note: *D* represents particle diameter.

This observation suggests that the flocculation effect of PVAc on chalcopyrite is weak, as it is not effective in enhancing the aggregation or increasing the particle size of chalcopyrite. PVAc has limited ability to promote the flocculation of chalcopyrite particles, which may be attributed to the mineral's surface properties that are less conducive to adsorption by PVAc. Furthermore, EDS spectral analysis of the chalcopyrite surface (Fig. 6a2–a6 and b2–b6) shows that the native chalcopyrite exhibits a relatively uniform distribution of Fe, S, Cu, and C elements, while O is sparsely distributed, likely due to slight surface oxidation. After interaction with PVAc, the distribution of Fe, S, Cu, and C on the chalcopyrite surface remains unchanged. Although a small amount of granular matter appeared in the distribution of O elements on the surface of the chalcopyrite, this is attributed to the adsorption of a few fine particles. Overall, the elemental content of Fe, S, Cu, C, and O on the chalcopyrite surface shows no significant variation. As an organic compound, carbon is a key element of PVAc. However, after interaction with PVAc, the carbon content on the chalcopyrite surface does not increase, indicating that there is no noticeable carbon accumulation. This suggests that the interaction between PVAc and chalcopyrite is minimal.

On the other hand, Fig. 7 provides a comparison of the SEM images and EDS spectra of natural talc and talc treated with PVAc. Fig. 7a1 shows that natural talc particles are relatively dispersed

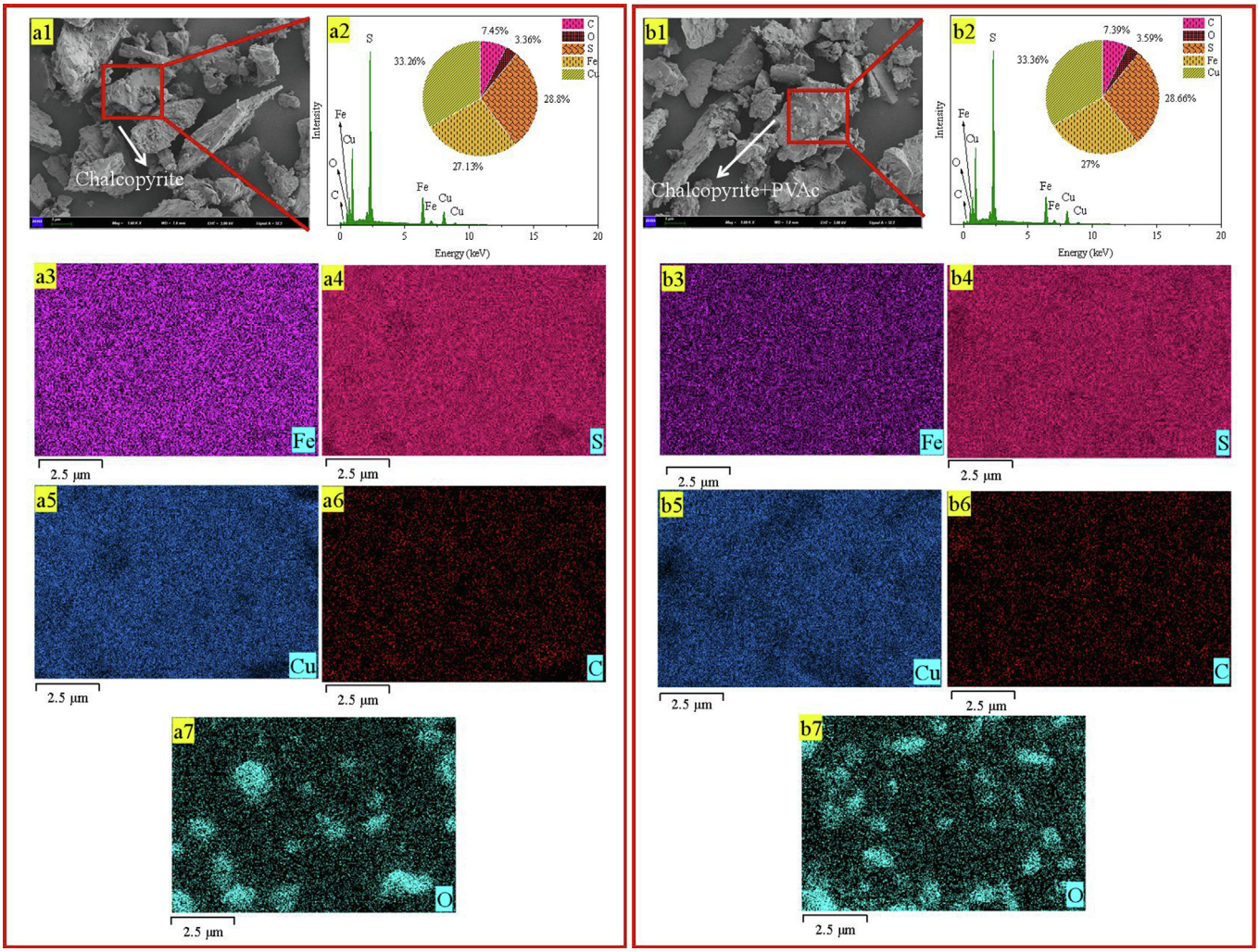


**Fig. 6.** SEM image of natural chalcopyrite (a1) and surface EDS elemental analysis of the magnified region (a2–a6), SEM image of chalcopyrite after reaction with PVAc (b1) and surface EDS elemental analysis of the magnified region (b2–b6) (pH: 8, and PVAc: 40 mg/L).

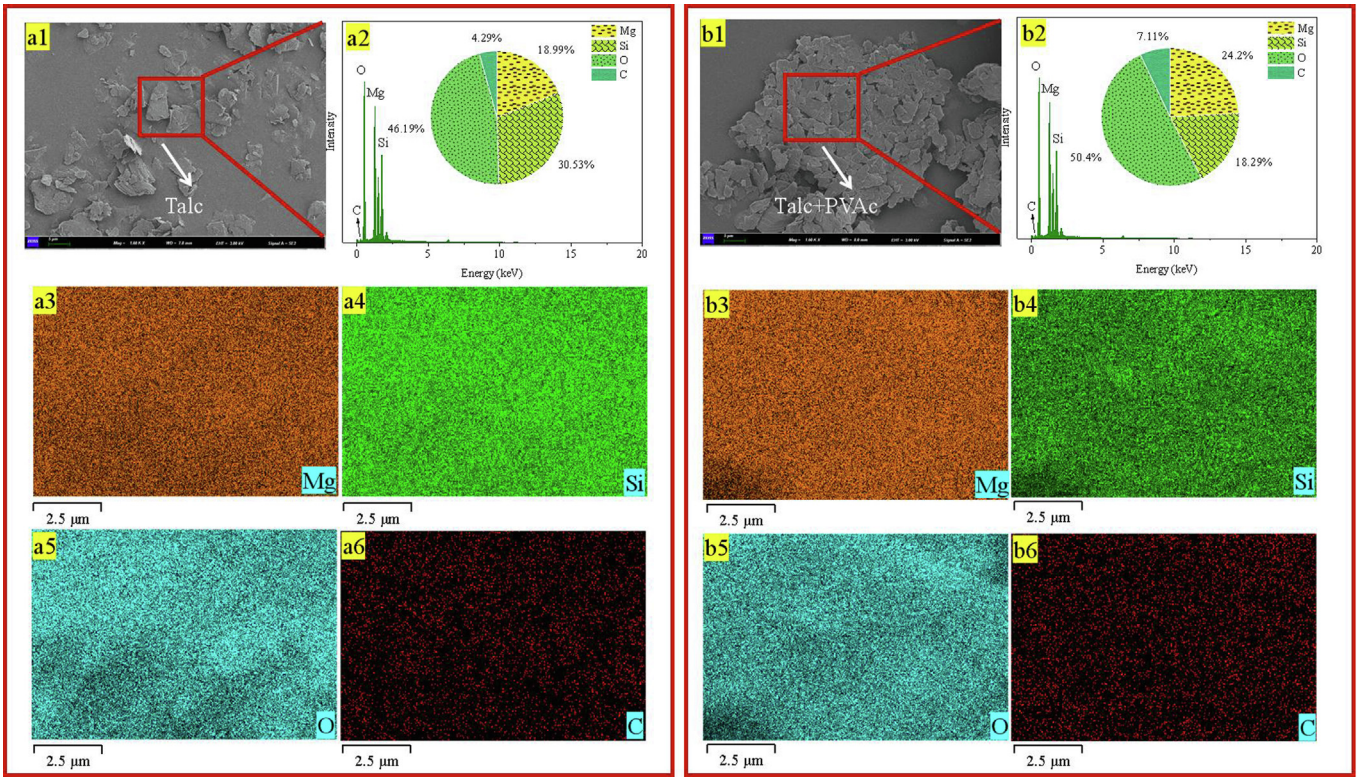


**Fig. 7.** SEM image of natural talc (a1) and surface EDS elemental analysis of the magnified region (a2–a6), SEM image of talc after reaction with PVAc (b1) and surface EDS elemental analysis of the magnified region (b2–b6) (pH: 8, and PVAc: 40 mg/L).

and primarily exhibit a flaky distribution with small particle sizes. These characteristics are typical of ultrafine talc, which has a tendency to remain dispersed in aqueous systems [21]. However, following treatment with PVAc, as shown in Fig. 7b1, the talc particles exhibit significant aggregation, forming compact talc flocs with a considerable increase in particle size. The overall morphology of the flocs is much more compact compared to the natural talc particles, indicating that PVAc has a strong and effective flocculation effect on ultrafine talc. This aggregation significantly increases the apparent particle size of talc, which is crucial for improving the flotation recovery of talc during the separation process. These results highlight the strong selective flocculation ability of PVAc, as it specifically enhances the aggregation of ultrafine talc particles without significantly affecting the chalcopyrite particles.

Furthermore, a comparison of the EDS spectra of natural talc (Fig. 7a2–a6) and talc treated with PVAc (Fig. 7b2–b6) reveals a notable increase in the carbon content on the surface of talc after interaction with PVAc. The natural talc surface contains a relatively low carbon content of 4.29%, which increases to 7.11% after PVAc treatment. This significant increase in carbon content suggests that PVAc, being an organic polymer, effectively adsorbs onto the surface of talc particles. The observed accumulation of carbon content on the talc surface provides direct evidence of the interaction between PVAc and talc, thereby further substantiating the conclusion that PVAc plays a crucial role in the flocculation and aggregation of ultrafine talc.

The analysis of surface morphology changes in chalcopyrite and ultrafine talc before and after PVAc treatment highlights the selective flocculation characteristics of PVAc. While PVAc has limited effect on chalcopyrite, it significantly enhances the aggregation and particle size of ultrafine talc, making it a highly effective flocculant for talc in the flotation separation process.

### 3.4. XPS analysis

Based on the results from laser particle size distribution measurements and SEM-EDS analyses, it can be concluded that PVAc exhibits a pronounced selective flocculation ability between chalcopyrite and ultrafine talc. In order to gain a deeper understanding of the mechanism underlying this selective behavior, XPS analyses were performed on both minerals prior to and following PVAc treatment. Fig. 8 displays the corresponding spectra and quantitative outcomes.

Referring to Fig. 8a, the XPS spectrum of natural chalcopyrite clearly reveals the presence of characteristic peaks corresponding to carbon (C), oxygen (O), copper (Cu), iron (Fe), and sulfur (S) elements, which are consistent with the expected surface composition of chalcopyrite. Further quantitative analysis (Fig. 8b) indicates that the atomic concentrations of C, O, Cu, Fe, and S are 25.61%, 23.38%, 17.18%, 7.32%, and 26.51%, respectively. After treatment with PVAc, however, there is no significant change in the contents of these surface elements compared with the untreated chalcopyrite sample. The main elements on the chalcopyrite surface are Cu, Fe, S, and O. During the interaction between chalcopyrite and PVAc, these elements could potentially serve as active sites for PVAc adsorption. To further investigate this, high-resolution spectra of Cu, Fe, S, and O were analyzed prior to and following PVAc treatment, as shown in Fig. S3 in the Supplementary Material. As illustrated, the binding energies of Cu 2p, Fe 2p, S 2p, and O 1s remain almost unchanged after PVAc treatment, indicating that there are no available adsorption sites for PVAc on the chalcopyrite surface.

PVAc does not strongly interact with the chalcopyrite surface and is not effectively adsorbed under the tested conditions [22]. Consequently, the inability of PVAc to promote flocculation of chalcopyrite can be primarily attributed to the lack of adsorption sites,

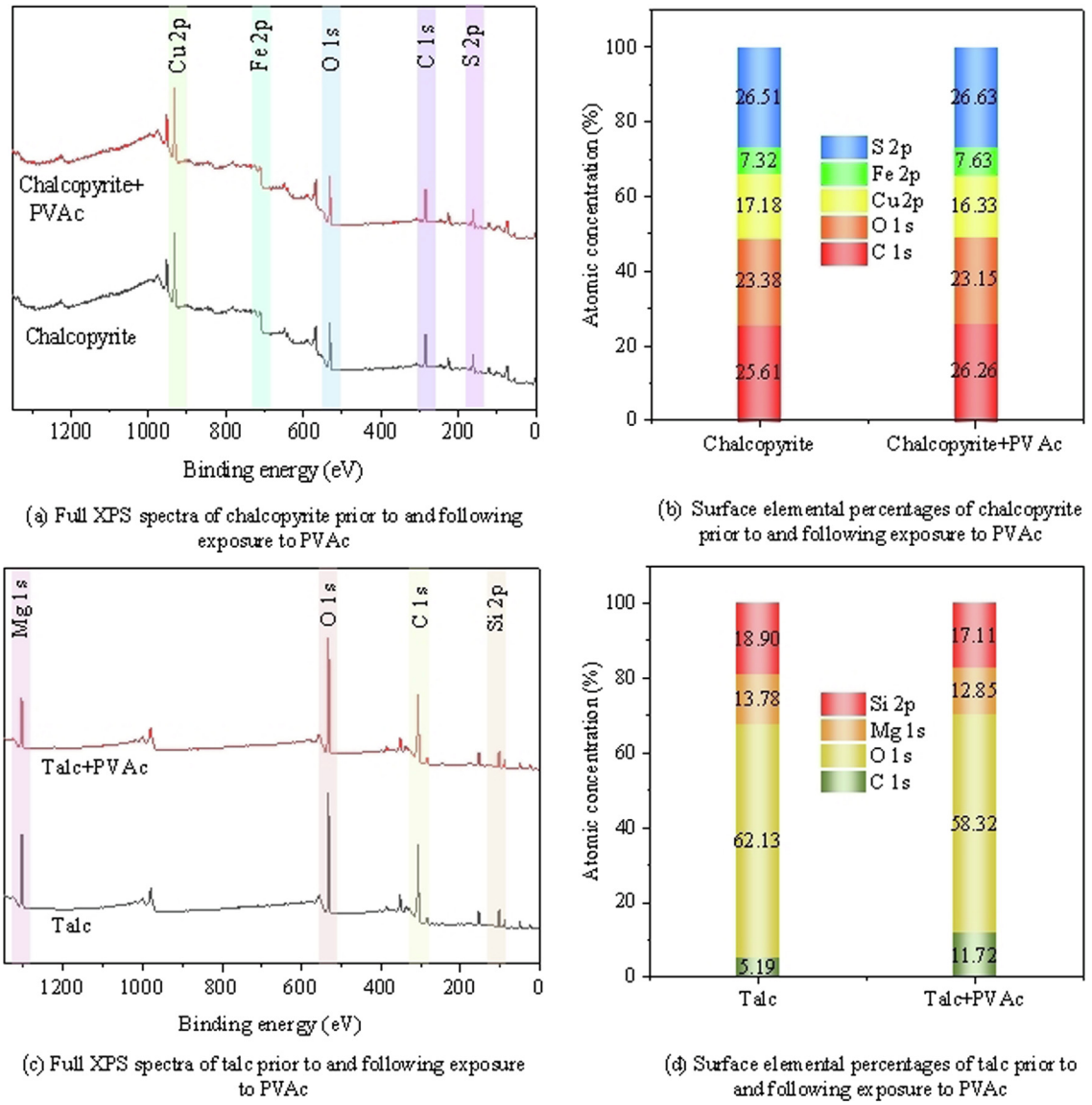


**Fig. 8.** Full XPS spectra of chalcopyrite and talc before and after PVAc treatment (pH: 8, and PVAc: 40 mg/L).

thereby preventing any meaningful change in the aggregation behavior of chalcopyrite particles.

The XPS analysis of talc before and after PVAc interaction, shown in Fig. 8c, presents a different scenario. On the natural talc surface, clear peaks corresponding to C 1s, O 1s, Mg 1s, and Si 2p are observed, aligning with the chemical composition of talc. As summarized in Fig. 8d, the atomic concentrations of C, O, Mg, and Si are measured at 5.19%, 62.13%, 13.78%, and 18.90%, respectively. The minor carbon content detected on the natural talc surface is likely attributable to surface contamination by atmospheric hydrocarbons, which is a common artifact in XPS measurements. Subsequent to the treatment by PVAc, a substantial growth of the carbon content was observed, with the atomic percentage rising from 5.19% to 11.72%. This notable increment in surface carbon concentration is consistent with the EDS findings and is a direct indication of PVAc adsorption onto the talc surface. Considering that PVAc is an organic compound with a high carbon content, the significant increase confirms the effective adsorption of PVAc on talc surfaces.

Building on this, the high-resolution XPS spectra of C, O, Mg, and Si on the talc surface before and after PVAc treatment were further analyzed and these spectra are shown in Fig. 9.

As shown in Fig. 9a, the C 1s peak of natural talc appears at 284.80 eV, corresponding to the reference carbon used for binding energy calibration. After interaction with PVAc, the deconvoluted C 1s spectrum showed three peaks at 284.80, 286.30, and 288.89 eV. Among them, the new peaks at 286.30 and 288.89 eV correspond to specific carbon atoms within the ester group (–COOR): 286.30 eV is attributed to the C–O bond (alkoxy carbon), while 288.89 eV corresponds to the carbon in the C==O (carbonyl) group [9,23]. This indicates that ester groups in PVAc are adsorbed onto the talc surface following their interaction. From the fitted O 1s, Mg 1s, and Si 2p spectra shown in Fig. 9b–d, it is observed that only the O 1s peak exhibits a slight shift of –0.34 eV after PVAc treatment, while the binding energies of Mg 1s and Si 2p remain unchanged. This suggests that the chemical environment of O changes slightly due to ester group interaction, but no new O 1s peak appears. Notably, binding energy shifts associated with chemisorption typically exceed 0.5 eV. Therefore, the observed shift of only 0.34 eV implies that PVAc adsorption on talc is not chemisorption, but rather characteristic of hydrogen bonding as physisorption [24].

These findings highlight a crucial distinction between the two minerals: while PVAc exhibits minimal interaction with

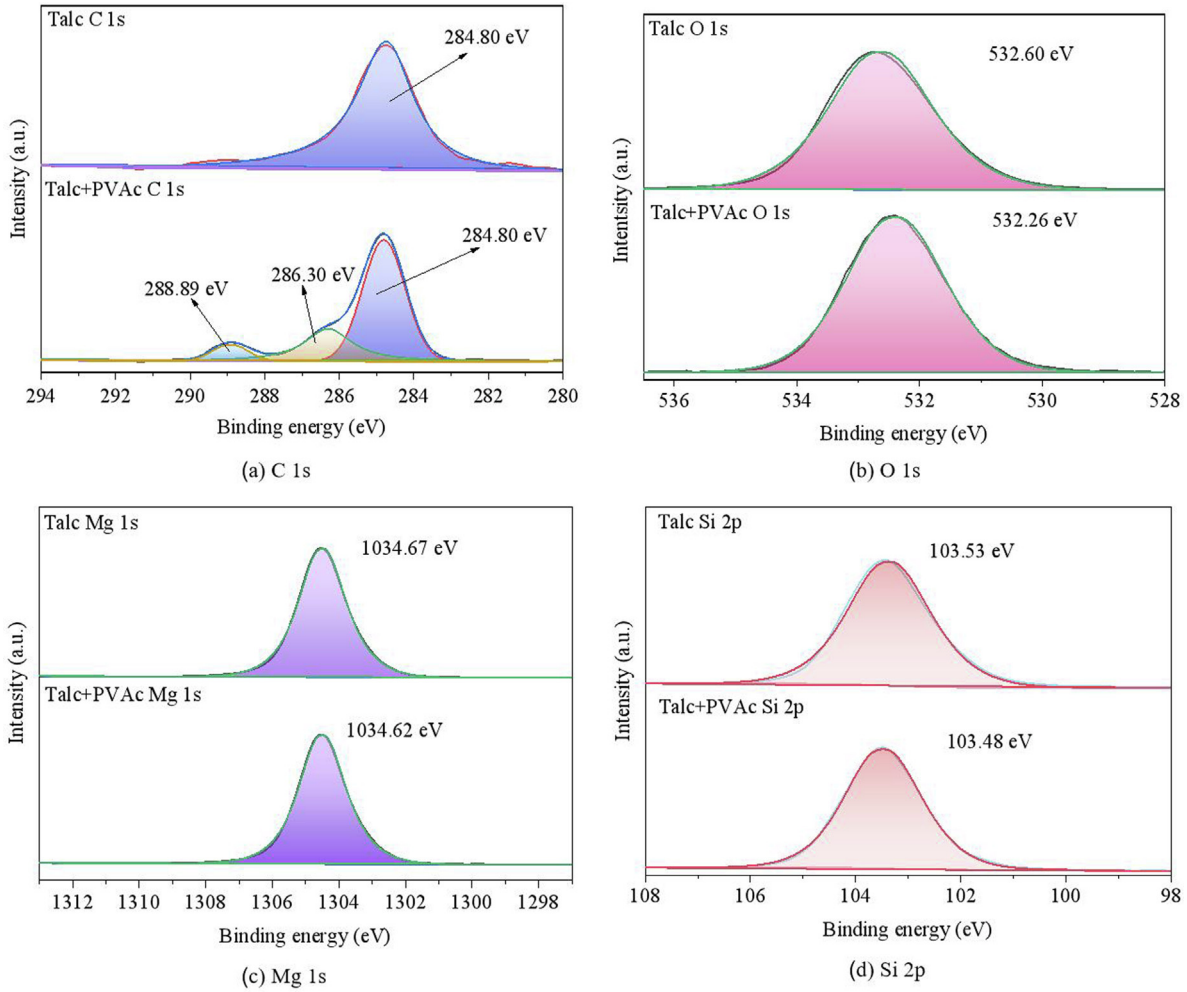


**Fig. 9.** High-resolution XPS spectra of talc before and after PVAc treatment (pH: 8, and PVAc: 40 mg/L).

chalcopyrite, it strongly adsorbs onto ultrafine talc, leading to selective flocculation. The selective adsorption behavior can be attributed to differences in surface properties. This selective adsorption ultimately governs the efficiency of PVAc in promoting flocculation of ultrafine talc particles while leaving chalcopyrite largely unaffected, thereby providing a basis for achieving effective reverse flotation separation in mineral processing applications.

### 3.5. DFT calculation analysis

To reveal the selective adsorption process of PVAc with chalcopyrite and talc, DFT calculations were performed to evaluate the adsorption energies and structural changes of PVAc on chalcopyrite and talc surfaces. The adsorption configurations are presented in Fig. 10.

As shown in Figs. 10a and c, the initial bond distances between the oxygen atoms of PVAc and the chalcopyrite and talc surfaces were measured at 2.67 and 2.61 Å, respectively, indicating the proximity of PVAc to both surfaces. After optimization of the structure (Figs. 10b and d), the O surface distance on chalcopyrite grew to 2.71 Å (Fig. 10b), implying that PVAc moved further from the chalcopyrite surface. This suggests a weak interaction between PVAc and chalcopyrite, making adsorption unfavorable [25]. In contrast, on the optimized talc adsorption configuration, the O atom in PVAc moved closer to the H atom on the talc surface, shortening the bond length from 2.61 to 1.90 Å (Fig. 10d). This indicates a stronger interaction between PVAc and talc, attributed to hydrogen bonding between the ester group of PVAc and surface H atoms on talc, leading to physical adsorption.

The calculated adsorption energies of PVAc on chalcopyrite and talc are listed in Table 1. PVAc exhibited a positive adsorption energy of +110.36 eV on the chalcopyrite (112) surface, indicative of a repulsive interaction that discourages adsorption. Conversely, the adsorption energy on the talc (001) surface was −0.35 eV, indicating a spontaneous and favorable adsorption process [26]. These findings corroborate the selective affinity of PVAc for talc over chalcopyrite. The presence of surface hydrogen atoms on talc provides active sites for hydrogen bond formation with PVAc, whereas the chalcopyrite surface lacks such sites, preventing strong interactions [27]. Therefore, the selective adsorption of PVAc onto talc rather than chalcopyrite underpins its effectiveness in selectively flocculating ultrafine talc particles while leaving chalcopyrite relatively dispersed [28].

### 3.6. Coverage angle test of flocculation

In the mineral flotation process, the key to particle recovery lies in the attachment of particles to bubbles. To further compare, at the microscopic level, the capture efficiency between ultrafine talc particles and bubbles before and after flocculation, a coverage angle measurement was conducted to simulate the particle–bubble interaction [29]. The findings are presented in Fig. 11.

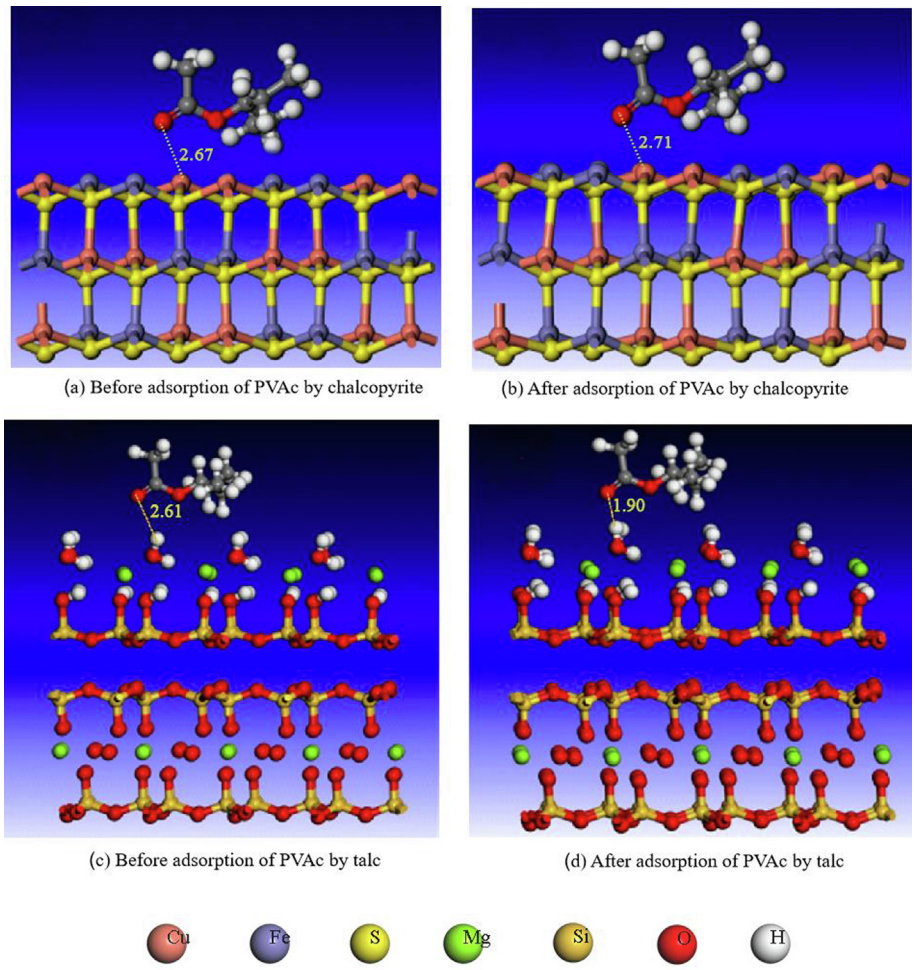


**Fig. 10.** The adsorption of PVAc on chalcopyrite and talc.
Note: (a) and (c) represent the configurations of PVAc prior to adsorption on the chalcopyrite (112) and talc (001) surfaces, respectively, whereas (b) and (d) the configurations following optimization.

**Table 1**
The adsorption energies of chalcopyrite and talc surfaces with PVAc.

| Adsorption models | $E_{Mineral}$ (eV) | $E_{Ragents}$ (eV) | $E_{Total}$ (eV) | $\Delta E$ (eV) |
|---|---|---|---|---|
| Chalcopyrite (112) + PVAc | −70051.49 | −2062.63 | −72003.76 | +110.36 |
| Talc (001) + PVAc | −81254.03 | −2062.63 | −83317.01 | −0.35 |

As shown in Fig. 11, the coverage angles between ultrafine talc and the bubble after 15 and 30 s of collision were 19.25° and 40.53°, respectively. In contrast, for talc flocs, the coverage angles reached 48.16° and 77.68° after 15 and 30 s of interaction with the bubble, respectively.

This comparison clearly demonstrates that, under identical collision times, the coverage angle between talc flocs and bubbles is significantly larger than that between individual ultrafine talc particles and bubbles. A larger coverage angle indicates a more extensive contact area, which is crucial for stable bubble-particle attachment. The formation of talc flocs effectively increases the apparent particle size and enhances the probability of collision with bubbles. Consequently, this structural change promotes more efficient attachment processes, thereby markedly improving the bubble-particle capture efficiency. These findings highlight the critical role of floc formation in optimizing particle-bubble interactions and, ultimately, in enhancing the separation performance in flotation systems [30].

This accounts for the improved flotation performance of talc flocs. In contrast, the poor floatability of ultrafine talc is primarily due to its extremely fine particle size, which limits effective collision and adhesion with bubbles [31].

### 3.7. Bubble-particle interaction calculations

Ultrafine talc particles are characterized by small size, low volume, and low mass. During flotation, ultrafine talc exhibits a comparatively weak interaction with bubbles, resulting in insufficient kinetic energy for effective collision and adhesion. Consequently, ultrafine talc particles cannot be efficiently captured by bubbles. However, once ultrafine talc is flocculated by PVAc, the apparent particle size and floatability of the talc flocs are significantly increased, leading to a notable enhancement in their interaction energy with bubbles during flotation.

To investigate the interaction between talc and bubbles, the interaction energy before and after talc flocculation was calculated using the classical extended DLVO theory.

The classical extended DLVO theory describes the interaction energy between mineral particles and bubbles, including van der

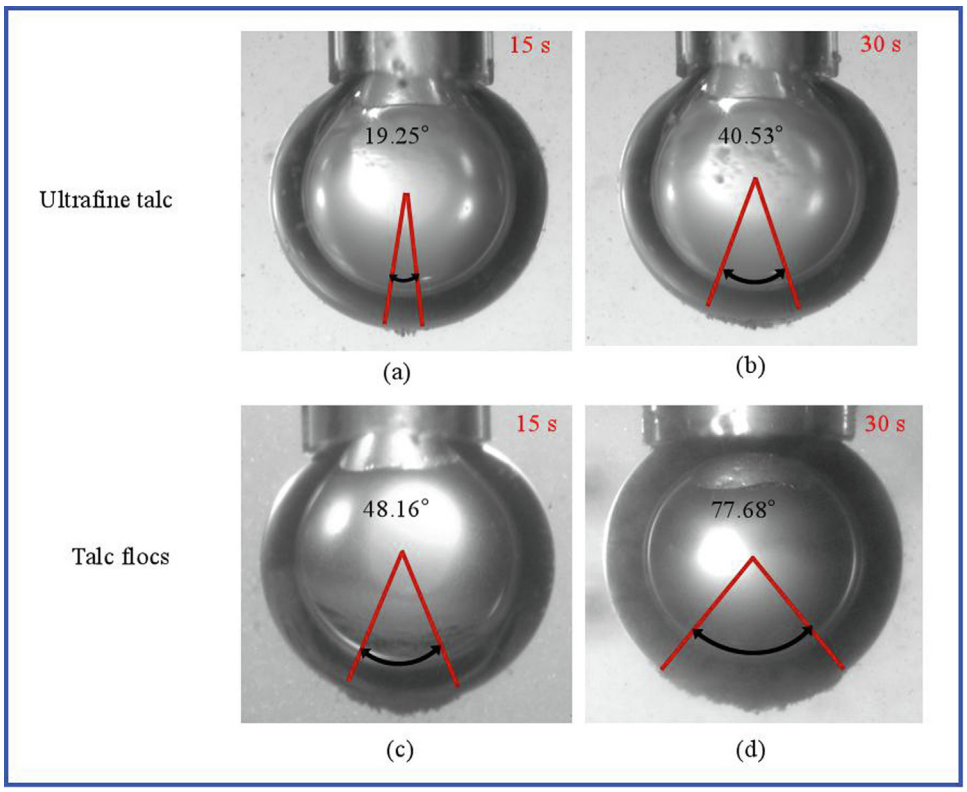


**Fig. 11.** Visualization results: Coverage angles between bubbles and ultrafine talc or talc flocs under different conditions.

Waals ($E_a$), electrostatic ($E_e$), and hydrophobic potential energy ($E_h$) [32,33]. In the calculation of interaction energy between ultrafine talc particles and bubbles before and after flocculation, both ultrafine talc particles and talc flocs are treated as ideal spherical particles with smooth surfaces and uniform chemical properties. The van der Waals interaction potential is given by:

$$E_a = -\frac{A_{132}}{6H} \times \frac{R_p R_b}{R_p + R_b} \tag{3}$$

$$A_{132} = \left(\sqrt{A_{11}} - \sqrt{A_{33}}\right) \times \left(\sqrt{A_{22}} - \sqrt{A_{33}}\right) \tag{4}$$

where $A_{132}$ represents the Hamaker constant of talc particles and bubbles in aqueous medium; $A_{11}$, $A_{22}$, and $A_{33}$ the Hamaker constants of particles, bubbles, and water in vacuum, respectively, which are $4.52\times10^{-20}$, 0, and $3.70\times10^{-20}$ J, respectively; $R_p$ and $R_b$ the radius of particles and particles/bubbles, where the radius $R_b$ of the bubble is 500 μm; and $H$ (mm) the separation distance. According to Section 3.3, the average particle size of the ultrafine talc is 7.34 μm, and the average particle size of the flocculated talc is 33.74 μm. Therefore, in the extended DLVO calculation, $R_p$ is taken as 3.67 and 16.87 μm, respectively.

The potential energy $E_e$ of electrostatic interaction between particles and bubbles can be calculated by Eqs. (5)–(7) [34].

$$E_e = \frac{\pi \varepsilon_0 \varepsilon_r R_p R_b}{R_p + R_b} (\varphi_1^2 + \varphi_2^2) \left[\frac{2\varphi_1 \varphi_2}{\varphi_1^2 + \varphi_2^2} p + q\right] \tag{5}$$

$$p = \ln\left[\frac{1 + \exp(-\kappa H)}{1 - \exp(-\kappa H)}\right] \tag{6}$$

$$q = \ln[1 - \exp(-2\kappa H)] \tag{7}$$

where $\phi_1$ and $\phi_2$ are the surface potentials of particles and bubbles, respectively, which are usually approximated by the zeta potential. According to the zeta potential data presented in Fig. 12a, the surface potential of ultrafine talc at pH 8 is –36.30 mV which shifts to –17.10 mV after treatment with the flocculant PVAc [35]. Therefore, in extended DLVO theory calculations, the surface potentials of ultrafine talc and talc flocs are taken as –36.30 and –17.10 mV, respectively, while the surface potential of bubbles remains at –32.78 mV [36]. The vacuum dielectric constant $\varepsilon_0 = 8.85 \times 10^{-12} \cdot \mathrm{F \cdot m^{-1}}$, relative permittivity of water $\varepsilon_r$=78.5 $\mathrm{C^2 \cdot J^{-1} \cdot m^{-1}}$, and $\kappa^{-1}$ (0.104 nm) is the Debye length in a 1 mM KCl solution.

The hydrophobic interaction energy $E_h$ can be calculated by Eqs. (8)–(10) [37].

$$E_h = -2.51 \times 10^{-3} \times \frac{R_p R_b}{R_p + R_b} \times h_0 k_1 \exp\left(-\frac{H}{h_0}\right) \tag{8}$$

$$h_0 = (12.2 \pm 1.0) k_1 \tag{9}$$

$$k_1 = \frac{\exp(\frac{\theta}{100}) - 1}{e - 1} \tag{10}$$

where $k_1$ denotes the partial hydrophobicity coefficient; $h_0$ the decay length, nm; and $\theta$ the contact angle of talc before and after interaction with PVAc. As shown by the water contact angle measurements in Fig. 12b, the contact angle of ultrafine talc is 42.00°, while the contact angle of talc flocs formed after interaction with PVAc increases to 56.00°.

$E_t$ is the total interaction energy between particles and bubbles, calculated using Eq. (11).

$$E_t = E_a + E_e + E_h \tag{11}$$

Based on the extended DLVO theory, the interaction energies between ultrafine talc and bubbles before and after flocculation were calculated, and the outcomes can be observed in Figs. 12c and d.

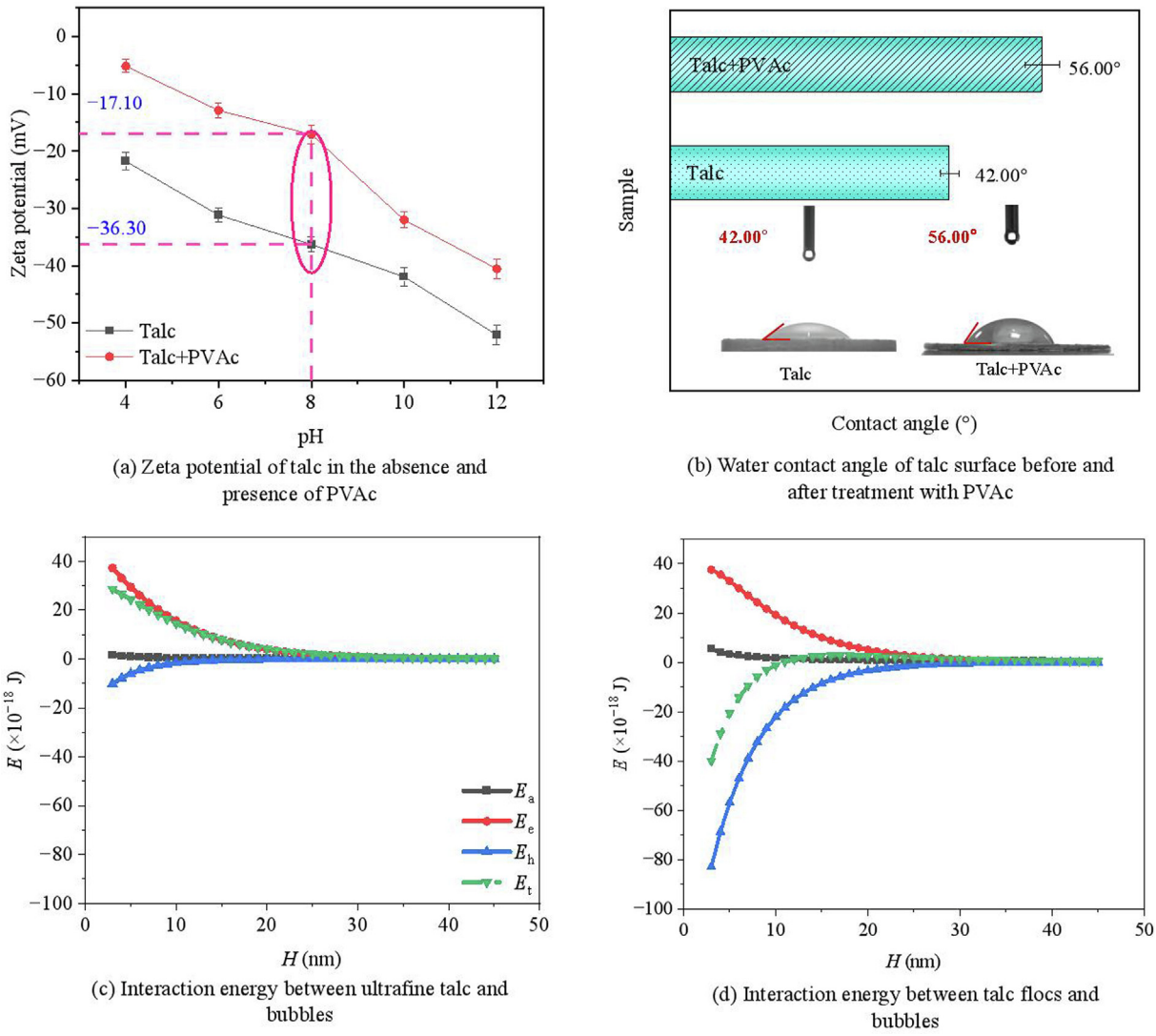


(a) Zeta potential of talc in the absence and presence of PVAc

(b) Water contact angle of talc surface before and after treatment with PVAc

(c) Interaction energy between ultrafine talc and bubbles

(d) Interaction energy between talc flocs and bubbles

**Fig. 12.** EDLVO interaction energy between ultrafine talc particles and talc flocs with bubbles (pH: 8, and PVAc: 40 mg/L).

In the extended DLVO theory calculation of particle-bubble interaction, when the total interaction energy $E_t$ is positive, it indicates a repulsive force between the particle and the bubble, making it difficult for the particle to adsorb onto the bubble. When the total interaction energy $E_t$ is negative, an attractive force exists between the particle and the bubble [38]. Fig. 12 shows the interaction energy between ultrafine talc and bubbles before and after talc flocculation by PVAc. As seen in Fig. 12a, before adding the flocculant PVAc, the interaction energy between ultrafine talc and the bubble is dominated by the electrostatic potential energy $E_e$, which is positive. Although the hydrophobic interaction energy $E_h$ is negative, its absolute value is relatively small, and the limited hydrophobic interaction results in the overall energy $E_t$ remaining positive. This indicates that the interaction between the mineral and the bubble is mainly repulsive, making it difficult for ultrafine talc to be effectively captured and adhered to the bubble, resulting in poor flotation ability of ultrafine talc [36].

After ultrafine talc interacts with PVAc, it is effectively flocculated, forming talc flocs with a significant increase in particle/floc size. Additionally, due to the hydrophobic effect of PVAc, the hydrophobicity of the flocs is also enhanced. Fig. 12b shows the interaction energy between the talc flocs and the bubble. As seen in Fig. 12b, after flocculation, the interaction energy between talc and the bubble is mainly governed by the hydrophobic interaction energy $E_h$. Since $E_h$ is negative and its magnitude has significantly increased, the total interaction energy $E_t$ between the flocculated talc and the bubble changes from positive to negative, and the interaction force between the talc and the bubble shifts from repulsive to attractive [39]. The enhanced attractive interaction between the flocs and the bubble increases the likelihood of effective collision and adhesion, leading to a significantly higher probability of bubble capture. This is the fundamental reason for the significant improvement in the flotation ability of talc after flocculation with PVAc [40].

## 4. Conclusions

This work is the first to investigate the use of the thermoplastic polymer PVAc as an effective hydrophobic and selective flocculant. The selective floc-flotation behavior of PVAc toward chalcopyrite and ultrafine talc was explored, aiming to contribute to the resource recovery from chalcopyrite tailings and to broaden the potential applications of PVAc in future mineral recovery processes. Single-mineral and artificial mixed ore experiments were conducted to examine the role of PVAc in the flotation separation of chalcopyrite and ultrafine talc. The selective flocculation and

adsorption mechanisms of PVAc on these minerals were analyzed. Additionally, this study explores the coupling mechanism between flocculation and flotation of ultrafine talc from a novel perspective, clarifying the interaction and capture processes between ultrafine talc and bubbles before and after flocculation. The key findings of this work are summarized below:

(1) Floc-flotation experiments confirmed that the thermoplastic polymer PVAc can serve as an efficient selective flocculant for the separation of chalcopyrite from ultrafine talc. The enrichment ratio of chalcopyrite concentrate was markedly improved from 1.32 to 1.76 with the addition of 40 mg/L PVAc under reverse flotation conditions, relative to conventional froth flotation without PVAc.
(2) Laser particle size and SEM-EDS analyses demonstrated that PVAc exhibits excellent selective flocculation, effectively adsorbing on the surface of talc particles. This promotes aggregation and the formation of talc flocs and increases the apparent particle size of ultrafine talc, while PVAc has almost no flocculation effect on chalcopyrite.
(3) XPS analysis and DFT calculations confirmed that the ester groups in PVAc interact with the hydrogen atoms on the talc surface through hydrogen bonding, resulting in PVAc adsorption onto talc. This enhances the hydrophobicity and floatability of talc, while there are no active sites on the chalcopyrite surface for PVAc to interact with, preventing PVAc adsorption on chalcopyrite.
(4) The coverage angle test revealed that compared with ultrafine talc, the talc floc by PVAc forms a larger coverage angle on bubbles and has a higher efficiency of being captured by the bubbles. Extended DLVO theory calculations (under smooth, homogeneous particle conditions) further supported these findings, showing that flocculation by PVAc increased the hydrophobic interaction energy between ultrafine talc and bubbles, shifting the total interaction energy from repulsion to attraction. This enhanced interaction facilitates the capture of talc flocs by bubbles, thereby improving flotation performance.

## Acknowledgments

This work was supported by the National Natural Science Foundation of China (Nos. 52174239 and 52374259), the Program of China Scholarship Council (No. 202406080114), and Natural Sciences and Engineering Research Council of Canada (No. NSERC RGPIN 2024-04570).

## Supplementary material

Supplementary data to this article can be found online at https://doi.org/10.1016/j.ijmst.2025.08.016.

## References

[1] Li CW, Xu M, Xing YW, Zhang HJ, Peuker UA. Efficient separation of fine coal assisted by surface nanobubbles. Sep Purif Technol 2020;249:117163.
[2] Han GH, Du YF, Huang YF, Yang SZ, Wang WJ, Su SP, Liu BB. Efficient removal of hazardous benzohydroxamic acid (BHA) contaminants from the industrial beneficiation wastewaters by facile precipitation flotation process. Sep Purif Technol 2021;279:119718.
[3] You YH, Yang L, Sun XB, Chen H, Wang H, Wang NQ, Li SQ. Synthesized cationic starch grafted tannin as a novel flocculant for efficient microalgae harvesting. J Clean Prod 2022;344:131042.
[4] Mansor ES, Abdallah H, Shaban AM. Fabrication of high selectivity blend membranes based on polyvinyl alcohol for crystal violet dye removal. J Envir Chem Eng 2020;8(3).
[5] Tazehabadi MJM, Ansari M, Sabzevari A. Controlled synthesis of poly(vinyl alcohol)-poly(acrylic acid) copolymers via cobalt mediated radical polymerization of vinyl acetate initiated by V-70. J Mol Struct 2025;1331:141637.
[6] Yin WZ, Xie Y, Yao J, Song NB, Chen KQ, Yin XM. Study on the effect of flocculation morphology on the floatability of talc flocs and the adhesion mechanism with air bubbles. Miner Eng 2023;203:108317.
[7] Zhang HY, Cao QB, Yan Y, Zou H, Huang XG, Liu DW. Flotation separation of galena and chalcopyrite by using hydroxyl radicals from an $Fe^{2+}$/NaClO system as depressants. Appl Surf Sci 2025;686:162128.
[8] Niu FS, Chen YY, Zhang JX, Liu F, Wang ZY. Selective flocculation-flotation of ultrafine hematite from clay minerals under asynchronous flocculation regulation. Int J Min Sci Technol 2024;34(11):1563–74.
[9] Zhao Y, Yang SK, Wen H, Shen Z, Han FR. Adsorption behavior and selectivity mechanism of flotation reagents applied in ternary plastic mixtures. Waste Manag 2019;87:565–76.
[10] Cao SH, Yin WZ, Yang B, Zhu ZL, Sun HR, Sheng QY, Chen KQ. Insights into the influence of temperature on the adsorption behavior of sodium oleate and its response to flotation of quartz. Int J Min Sci Technol 2022;32(2):399–409.
[11] Xie Y, Yin WZ, Yao J, Xue FJ, Liu JY, Ban XQ. Application and mechanism of an efficient hydrophobic flocculant CPAM in the flocculation reverse flotation of hematite and microfine-grained chlorite. J Environ Chem Eng 2024;12(3):112608.
[12] Xie RQ, Tong X, Xie X, Zhu YM, Liu J. Flaxseed gum as new depressant in the separation of apatite and dolomite and its mechanism. Appl Surf Sci 2022;593:153390.
[13] Ajao V, Fokkink R, Leermakers F, Bruning H, Rijnaarts H, Temmink H. Bioflocculants from wastewater: Insights into adsorption affinity, flocculation mechanisms and mixed particle flocculation based on biopolymer size-fractionation. J Colloid Interface Sci 2021;581:533–44.
[14] Sun HR, Wang YL, Wang DW, Yao J, Yin WZ, Li MQ, Han HL, Yuan ZG. Selective control of surface characteristics of magnesite and quartz by a novel silicophilic collector stearylamine acetate. Appl Surf Sci 2025;680:161288.
[15] Sheng QY, Yin WZ, Yang B, Cao SH, Sun HR, Ma YQ, Chen KQ. Improving surface sulfidization of azurite with ammonium bisulfate and its contribution to sulfidization flotation. Miner Eng 2021;171:107072.
[16] Zhan WQ, Yang SY, Bao SX, Ren LY, Liu C. A novel insight of interaction mechanism of carboxymethyl cellulose with talc surface: A combined molecular dynamic simulation and DFT investigation. Appl Clay Sci 2024;247:107201.
[17] Ge WC, Liu J, Ren H, Zhu YM, Han WJ, Han YX. Enhanced mixed flotation of copper-molybdenum ore using dodecyl dimethyl betaine-emulsified kerosene as environmentally friendly collector. J Clean Prod 2024;447:141576.
[18] Li WB, Cheng SK, Zhou LB, Han YX. Enhanced iron recovery from magnetic separation of ultrafine specularite through polymer-bridging flocculation: A study of flocculation performance and mechanism. Sep Purif Technol 2023;308:122882.
[19] Hirajima T, Miki H, Suyantara GPW, Matsuoka H, Elmahdy AM, Sasaki K, Imaizumi Y, Kuroiwa S. Selective flotation of chalcopyrite and molybdenite with $H_2O_2$ oxidation. Miner Eng 2017;100:83–92.
[20] Wang C, Sun CB, Liu Q. Formation, breakage, and re-growth of quartz flocs generated by non-ionic high molecular weight polyacrylamide. Miner Eng 2020;157:106546.
[21] Peng WJ, Lv S, Cao YJ, Wang W, Liu SG, Huang YK, Fan GX. A novel pH-responsive flocculant for efficient separation and recovery of Cu and Mo from secondary resources via selective flocculation-flotation. J Clean Prod 2023;395:136463.
[22] Feng B, Zhang WP, Guo YT, Peng JX, Ning XH, Wang HH. Synergistic effect of acidified water glass and locust bean gum in the flotation of a refractory copper sulfide ore. J Clean Prod 2018;202:1077–84.
[23] Xu F, Wang SW, Yuan XL, Kong RJ. Effects of nonionic collectors with oxygen-containing functional groups on flotation performance of low-rank coal. Fuel 2022;330:125585.
[24] Zhang H, Chai WC, Cao YJ. Flotation separation of quartz from gypsum using benzyl quaternary ammonium salt as collector. Appl Surf Sci 2022;576:151834.
[25] Luo YJ, Ou LM, Chen JH, Zhang GF, Xia YQ, Zhu BH, Zhou HY. Mechanism insights into the hydrated Al ion adsorption on talc (001) basal surface: A DFT study. Surf Interfaces 2022;30:101973.
[26] Xie Y, Ban XQ, Yin WZ, Song NB, Yao J. The application of $KMnO_4$ in reverse flotation separation of chalcopyrite and talc and its selective depression mechanism. J Environ Chem Eng 2024;12(6):114429.
[27] Xie Y, Yin WZ, Yao J, Yin XM, Liu JY, Xue FJ, Tian DL. Flotation behavior and surface adsorption mechanism of a novel selective inhibitor HDP in the separation of chalcopyrite and talc flotation. J Mol Liq 2024;398:124206.
[28] Sun XS, Ma XM, Fan YP, Dong XS, Chang M, Feng ZY, Peng DQ. Insight into filter cake characteristics offine coal tailings assisted by CPAM and α-HH during pressure filtration. Sep Purif Technol 2023;326:124822.
[29] Tong Z, Dong LS, Wang XX, Bu XN. Enhancement mechanism of the difference of hydrophobicity between anode and cathode active materials from spent lithium-ion battery using plasma modification. ACS Sustain Chem Eng 2024;12(22):8541–51.
[30] Ren LY, Zhang ZY, Zeng WN, Zhang YM. Adhesion between nanobubbles and fine cassiterite particles. Int J Min Sci Technol 2023;33(4):503–9.

[31] Yang DL, Zhao ZQ, Gong L, Sun YX, Peng XW, Peng QY, Wang T, Liu Q, Zhang H, Zeng HB. Surface interaction mechanisms of air bubbles, asphaltenes and oil drops in aqueous solutions with implications for interfacial engineering processes. J Colloid Interface Sci 2023;647:264–76.
[32] Chen SJ, Tang LF, Tao XX, He H, Yang Z, Chen L. Exploration on the mechanism of oily-bubble flotation of long-flame coal. Fuel 2018;216: 427–35.
[33] Xu J, Yu HQ, Li XY. Probing the contribution of extracellular polymeric substance fractions to activated-sludge bioflocculation using particle image velocimetry in combination with extended DLVO analysis. Chem Eng J 2016;303:627–35.
[34] Wu CD, Wang LX, Harbottle D, Masliyah J, Xu ZH. Studying bubble-particle interactions by zeta potential distribution analysis. J Colloid Interface Sci 2015;449:399–408.
[35] Zhang HY, Wang KP, Wang D, Li JQ, Xiang BL, Tan XL, Liu Q. Kaolinite surface charges developed in cyclohexane suspension with dissolved Span 80 or bitumen: Electrodeposition and adsorption/desorption studies. Chem Eng J 2023;473:145406.
[36] Yang B, Zhu LT, He JF, Fu YF, Yin WZ. Effective reverse flotation separation of siderite from hornblende using pentaethoxylated tallow amine as a selective collector. Appl Surf Sci 2023;638:158030.
[37] Wang WJ, Huang YF, Zuo JP, Kou LL, Liu BB, Sun H, Han GH. A feasible strategy for separating oxyanions-loaded microfine Fe-MOF adsorbents from solution by bubble flotation. Chem Eng J 2023;454:140299.
[38] Zeng LQ, Franks GV, Goudeli E. Aggregation and breakage dynamics of alumina particles under shear by coupled computational fluid dynamics-discrete element method. J Colloid Interface Sci 2024;661:750–60.
[39] Li M, Xia YC, Zhang YF, Ding SH, Rong GQ, Cao YJ, Xing YW, Gui XH. Mechanism of shale oil as an effective collector for oxidized coal flotation: From bubble-particle attachment and detachment point of view. Fuel 2019;255:115885.
[40] Yin WZ, Xie Y, Zhu ZL. Literature overview of basic characteristics and flotation laws of flocs. Int J Miner Metall Mater 2024;31(5):943–58.